Fluorescent foci quantitation for high-throughput analysis

Elena Ledesma-Fernández and Peter H. Thorpe*

The Francis Crick Institute, Mill Hill Laboratory, The Ridgeway, Mill Hill, London, United Kingdom NW71AA

*Corresponding author: Peter Thorpe, The Francis Crick Institute, Mill Hill Laboratory, The Ridgeway, Mill Hill, London, United Kingdom NW71AA.
Email: Peter.Thorpe@crick.ac.uk

Abstract A number of cellular proteins localize to discrete foci within cells, for example DNA repair proteins, microtubule organizing centers, P bodies or kinetochores. It is often possible to measure the fluorescence emission from tagged proteins within these foci as a surrogate for the concentration of that specific protein. We wished to develop tools that would allow quantitation of fluorescence foci intensities in high-throughput studies. As proof of principle we have examined the kinetochore, a large multi-subunit complex that is critical for the accurate segregation of chromosomes during cell division. Kinetochore perturbations lead to aneuploidy, which is a hallmark of cancer cells. Hence, understanding kinetochore homeostasis and regulation are important for a global understanding of cell division and genome integrity. The 16 budding yeast kinetochores colocalize within the nucleus to form a single focus. Here we have created a set of freely-available tools to allow high-throughput quantitation of kinetochore foci fluorescence. We use this 'FociQuant' tool to compare methods of kinetochore quantitation and we show proof of principle that FociQuant can be used to identify changes in kinetochore protein levels in a mutant that affects kinetochore function. This analysis can be applied to any protein that forms discrete foci in cells.

Keywords: kinetochore, fluorescence, yeast, cerevisiae, ImageJ

INTRODUCTION

The advent of genome-wide green fluorescence protein (GFP) labeling has enabled the location of most cellular proteins to be determined *in vivo* [1]. This type of study has revealed that, for a number of cellular processes, proteins colocalize to discrete foci either as part of their normal homeostasis or in response to specific stimuli [2,3]. For example, DNA repair proteins relocalize to discrete foci that are coincident with double strand breaks [4]. The study of these foci provides insight into the underlying biological processes (for example see [5]).

Kinetochores are specialized protein complexes that assemble on centromeres to direct the segregation of chromosomes during cell division [6-8]. Defects in kinetochore function result in errors in chromosome segregation, which lead to aneuploidy and genome instability, a hallmark of cancer cells [9-12]. Hence, altered levels of kinetochore proteins may disrupt normal chromosome segregation and play a role in tumorigenesis or tumor development. In support of this notion, over-expression of several kinetochore and checkpoint genes has been found in tumor cells [13-16]. For this reason, and to understand the basic structure of the kinetochore, a key question is to understand the assembly and homeostasis of kinetochores. However, assessing the levels of proteins that are specifically located at the centromere is relatively difficult. The total cellular protein levels are not indicative of the protein loaded onto the centromere (i.e. part of the kinetochore),

hence standard biochemical techniques are not necessarily informative. This question has been addressed in the yeast *Sacharomyces cerevisiae* by quantitatively assessing kinetochore protein levels using fluorescence imaging [17-20]. An advantage of budding yeast is that all 16 centromeres cluster together to a single focus within the yeast nucleus that approximates to a diffraction-limited spot. Hence, measuring the fluorescence intensity of these foci allows quantitative assessment of kinetochore protein levels. One of the next steps in understanding kinetochore biology is to understand how the levels of the kinetochore proteins change in response to perturbations such as mutations, over-expression of endogenous genes or drug treatments. This requires a high-throughput method of assessing kinetochore protein levels using fluorescence imaging. We have developed a modular script, 'FociQuant', written for the freely available ImageJ software that enables quantitation of the fluorescence intensity of kinetochore foci (or any other fluorescent foci). The script could be used for images of single cells, but it is designed to be used for high-throughput imaging approaches. We use FociQuant to compare established 2-dimensional and 3-dimensional quantitation methods and show that under normal conditions the reported approaches give well-correlated results. We also show that the data generated using FociQuant compares well with that obtained using commercial software. We assess the ability of FociQuant to detect changes in kinetochore protein levels between haploid and diploid cells and also those produced by a checkpoint mutant. We find that changes

in the fluorescence intensity of foci of yellow fluorescent protein (YFP) linked to kinetochore protein Dad4 in *mad1Δ* cells are detected using FociQuant. These data suggest that changes in kinetochore homeostasis can be used to identify mutants that lead to chromosomal instability. The software could be used to quantify other types of foci, such as those formed by centrosome proteins and we show proof of principle for simultaneously quantifying two different foci in the same images.

MATERIALS AND METHODS

Yeast strains used here are based either upon W303 *ADE2+ RAD5+* genetic background [21, 22] or for *MIF2-GFP* the BY4741 strain [23] grown using standard methods [24]. A fluorescently-tagged strain, T37, was generated via homologous recombination of a linear PCR product, to create endogenously tagged *DAD4-YFP* (*MAT**a** can1::STE2pr-Sp_his5 lyp1Δ::STE3pr-LEU2 DAD4-YFP::NATMX SPC42-RFP::HYGMX*) and this was used to derive PT146-1A (*MATα TRP1 lys2Δ DAD4-YFP::NATMX SPC42-RFP::HYGMX*). The homozygous diploid *DAD4-YFP/DAD4-YFP* strain, PT206, is a cross between T37 and PT146-1A. The heterozygous diploid strain PT207 contains only one tagged allele of *DAD4* (*MAT**a**/α trp1-1/TRP1 lys2Δ/LYS2 can1::STE2pr-Sp_his5/ can1-100 lyp1Δ::STE3pr-LEU2/LYP1 DAD4/DAD4-YFP::NATMX SPC42-RFP::HYGMX/SPC42)*. The deletion of *MAD1* was introduced by amplifying the *KANMX* cassette from the *mad1::KANMX* strain from the gene deletion library [25] and transforming this into T37 (genotype as T37 but with *mad1::KANMX*). For imaging Mtw1-YFP, haploid E66 (*MATα TRP1 lys2Δ MTW1-YFP*) and diploid PT6 (*MAT**a**/α trp1-1/ TRP1 lys2Δ/LYS2 BAR1/bar1::LEU2 MTW1-YFP/MTW1-YFP*) strains were used. The *MIF2-GFP* strain is from the GFP collection of strains [1] (*MAT**a** his3Δ1 leu2Δ0 met15Δ0 ura3Δ0 MIF2-GFP::HIS3MX*). We confirmed the sequence of modified loci using PCR and Sanger sequencing.

Yeast were prepared for imaging by growth in synthetic complete media at 23°C (containing 120 mg/L adenine to minimize the concentration of the autofluorescent adenine biosynthetic intermediate phosphoribosylamino-imidazole). Log-phase cells were mixed with low melting point agarose to 0.7% and placed on a glass microscope slide beneath a 22 mm square ~170 μm thick coverslip and imaged within 10 minutes. The depth of agarose between the slide and coverslip is fixed at 6-8 μm, slightly larger than the diameter of the average yeast cell, which maintains a consistent distance from the coverslip to the cell nucleus. Cells were imaged with a Zeiss Axioimager Z2 microscope (Carl Zeiss AG, Germany), using a 63 × 1.4 NA plan apochromat oil immersion lens. Zeiss Immersol 518F immersion oil was used with a refractive index of 1.5181. Fluorescence illumination was provided by a Zeiss Colibri LED illumination system (a 505 nm LED was used for YFP excitation, 470 nm was used for GFP illumination and 590 nm used for RFP illumination). Fluorescence emission passed through filter sets from Zeiss (60HE for YFP and RFP and 38HE for GFP). Brightfield contrast was enhanced with differential interference contrast (DIC) prisms. The resulting light was captured using a Hamamatsu Flash 4.0 Lte CMOS camera with 6.5 μm pixels, binned 2 × 2 (Hamamatsu Photonics, Japan). The exposure times were set to ensure that pixels were not saturated, typically 200 msec. The resulting 16-bit images have a pixel size of 206 nm in x and y and a z step size of 350 nm. Images shown in the figures were prepared using Volocity imaging software (Perkin Elmer Inc., USA) or ImageJ [26].

A

DIC image   YFP Fluorescence image

DIC   YFP   Merge

B
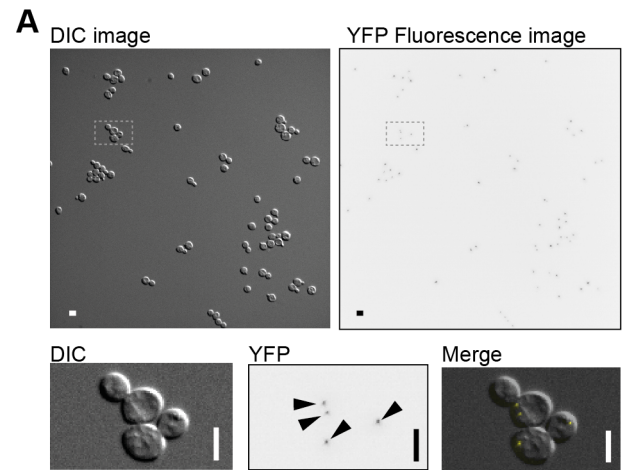
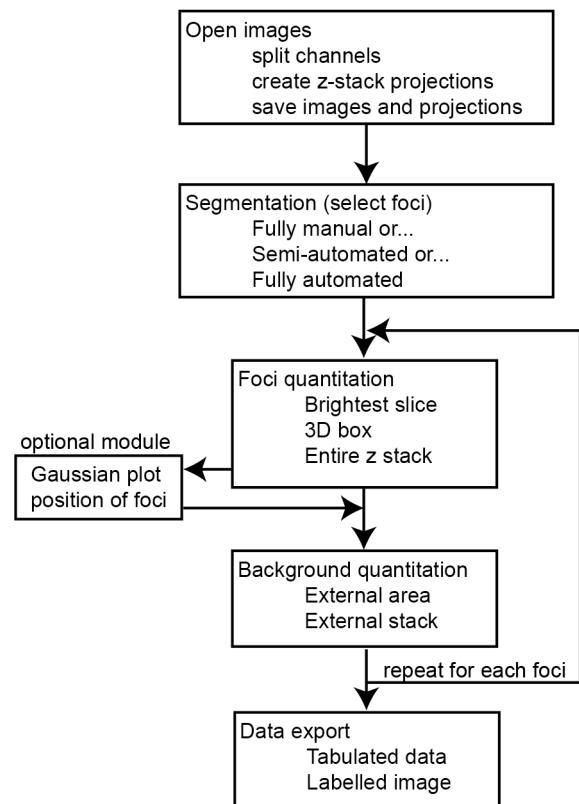## Sofware modules of foci quantitation

Figure 1. Outline of image analysis protocol. A. An image of fluorescently-tagged Dad4 (Dad4-YFP) highlights stereotypical kinetochore foci. The boxed region in the image is magnified and individual kinetochores are highlighted with arrowheads on the right. The scale bar in the micrographs is 5 μm. **B.** The flow chart illustrates the steps taken by the ImageJ script to quantify foci, each box indicates a separate module in the software.

RESULTS

A key requirement of quantifying fluorescent images is that the imaging system produces a linear relationship between the number of photons emitted from the sample and the voltage readout; often from a shift register (CCD) or active-pixel (CMOS) sensor. This relationship can be determined experimentally for any system and it is a prerequisite

of quantitative imaging. Space does not permit a full discussion of appropriate imaging systems, but this information is available elsewhere [27]. Specifically for kinetochore imaging, there are excellent resources for obtaining appropriate images that avoid many of the confounding issues associated with quantifying fluorescence [17] and the system used here is described further in the Materials and Methods. Images are typically either single channel (1 color, for example **Fig. 1A**) or multichannel (for example **Fig. 6D**) and contain a stack of images (a z stack) where each z slice is in a different plane of focus. As proof of principle we chose to use the kinetochore protein Dad4, a component of the microtubule-associated outer kinetochore DAM1/DASH complex [28]. We tagged this protein with YFP by fusing the endogenous *DAD4* gene to that encoding YFP. We wished to create a simple system of image quantitation that was robust and had the potential to be used with many images as part of a high-throughput approach. A number of commercial software and data analysis packages are available to enable quantitation, but we wished to develop an open access system that would use freely available software. To increase the flexibility of the system we also wanted to create a modular system that could incorporate additional features. We have made use of the popular ImageJ software, which is widely adopted and freely available [26], and we have developed a modular script (illustrated in **Fig. 1B**) that quantifies the fluorescence intensity of foci from 3 dimensional (3D) images. The script is divided into several simple modular algorithms and a detailed description of each module is provided in the supplementary information. A number of the modules are interchangeable to allow different parameters to be used in selecting foci or for including the quantitation of another channel of fluorescence emission. The script, including the individual modules is freely available to download (https://sourceforge.net/projects/fociquantitation/files/).

Segmentation

A typical kinetochore focus (**Fig. 2A**) is assumed to be a diffraction limited point source, although in reality the individual kinetochores are spaced in a region ≤ 200 nm [29]. In any case, the bulk of the fluorescence emission is contained within an x-y area consistent with the point spread function of the optical system (~550 nm for our system). Using a wide field imaging system the resolution in the z dimension is less precise and consequently the foci appear elongated in this dimension (**Fig. 2B**). A first step in quantifying these foci is to identify their x, y and z position in an image such as **Figure 1A**. There are a number of methods for identifying bright points in both 2-dimensional (2D) and 3D images (for example with CellProfiler [30] or FindFoci [31]). The method by which foci are identified has implications for the subsequent quantitation of the fluorescence signals. Cells growing asynchronously or mixed populations of cells may have foci that are fundamentally different in their fluorescence intensity. Kinetochore intensity increases during S phase as the centromeres are replicated and then decreases as the two sister kinetochores separate during mitosis. Furthermore, different mutants may have foci of different intensities or differing shapes. Therefore, our ImageJ script incorporates one of three different segmentation modules that allow foci to be selected in different ways. In each case the output is a set of points in each image that align in two dimensions (x and y) with each focus. A fully automated approach allows the user to set a specific noise threshold for the 'FindMaxima' process in ImageJ and then uses this to get a selection of points for each image. The advantage of this method is that it can be applied to multiple images without any manual intervention and consequently is suitable for high-throughput analysis. Automated segmentation is also
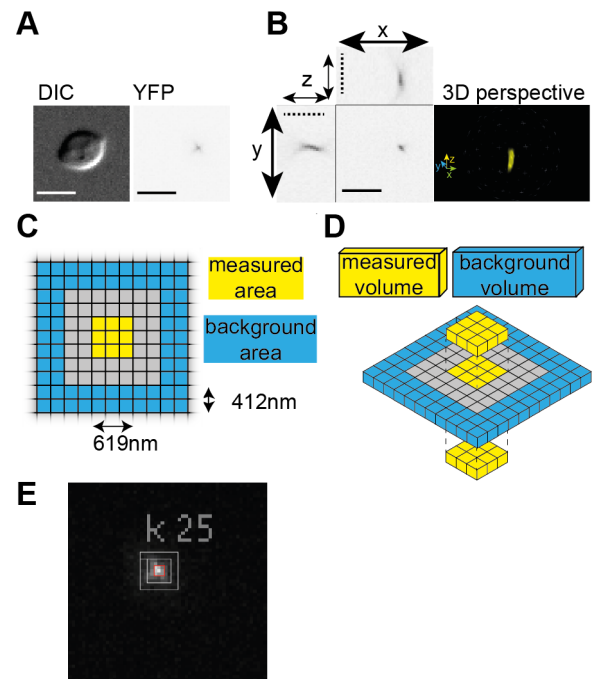

Figure 2. Quantitation of fluorescence foci. A. A typical kinetochore focus is shown in 2 dimensions, the scale bar is 5 μm. **B.** The focus has a third dimension in z that is extended due to the optical imaging system. The solid scale bar in x and y dimensions and dashed scale bar in z are all 5 μm. **C.** 2D quantitation measures a defined square of pixels (yellow 3 × 3 in this case) with a background region (blue) two pixels outside of the measured region. **D.** 3D quantitation measures the brightest z slice plus the z slices directly above and below this plane, although the background measurement remains a single z slice in the brightest plane. **E.** The graphical output from the software includes an image with all the measured objects indicated (a small region is shown here). The measured and background regions are indicated together with an identifying number, which can be used to track this particular object to specific measurements in the tabulated output (e.g. **Table S1**). The measured kinetochore and background regions have the dimensions illustrated in (C).

unbiased, since there is no user input. However, this type of segmentation suffers from a lack of precision, since there is no guarantee that only genuine kinetochore foci are selected. While it is possible to filter some aberrant measurements out of the resulting data using quantitative parameters, we wanted to create alternative selection methods. Therefore the second method allows the user to select the threshold manually for each image. This has the advantage that each focus does not need to be selected separately, instead the threshold is adjusted manually to an appropriate level that is optimum for each image. This semi-automated method would be ideal if the overall fluorescence intensity is very different between images, but consistent within an image. The third method allows the user to manually select each focus in each image. While this method is time consuming, it can reduce false positives if the user is readily able to select the correct foci in the image and can be applied to a subgroup of cells within a field of view. When using the manual selection method, the selected points do not need to exactly align with the center of the focus, since the quantitation module will then search locally for the brightest point (the size of this search area can be defined within the module). This manual segmentation is ideal if only specific cells within an image need to be quantified. The choice

of which segmentation method to employ should be determined either by the requirement to select only specific foci (the manual method) or the need to select all foci (the semi-automated/automated method).
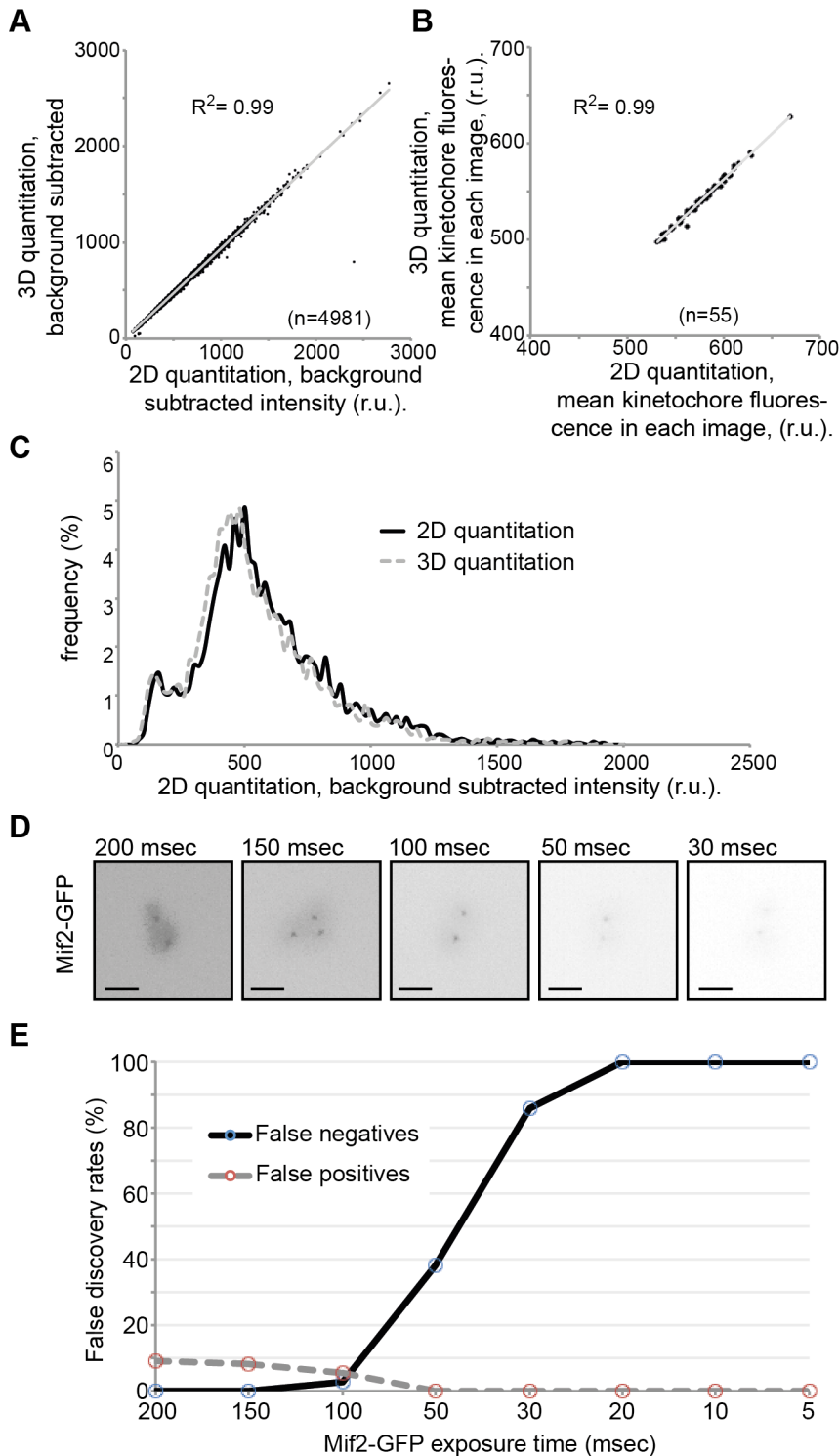

Figure 3. Comparing different types of fluorescence measurements. A. The 3D box measurement is compared with the 2D measurement for 4981 Dad4-YFP foci, the measurements correlate well. **B.** The 3D and 2D measurements also correlate for each image as a whole. The average kinetochore focus intensity for each of the 55 images are compared using the two methods. In both panel A and B, then mean intensities are shown rather than integrated intensities. **C.** The distribution of the 2D measurements is shown indicating a relatively broad distribution of intensities from the 4981 foci (with a mean intensity of 469 r.u.). The distribution of 3D measurements (dashed line) is very similar to that for the 2D measurements. All foci were selected using the fully automated method. All fluorescence measurements are expressed in relative units (r.u.). **D.** Different exposure times for Mif2-GFP images are shown with identical contrast, the scale bar is 5 µm. **E.** The false discovery rates were estimated from the Mif2-GFP images assuming that cells would contain either one or two foci. False positives indicate the automated detection of extra 'non-kinetochore' foci and false negatives indicate a failure to detect genuine kinetochore foci.

Quantitation

The primary aim of the FociQuant quantitation is to measure the intensity of the fluorescence and this is achieved in three ways, each of which is based upon common methods used in the literature. First, a square area around each focus (typically ~600 nm) is used as the x-y area for quantitation, sufficient to account for the majority of the fluorescence from kinetochores [18]. This area can be adjusted based upon the pixel size of the image (in our images each pixel is 206 nm square, consequently we used a 3 × 3 pixel square, **Fig. 2C**). Since each image is composed of a stack of vertically separated images (z stack), the script next identifies the brightest z slice within the z stack. Assuming that this brightest square is not at the very top or bottom of the z stack, the mean intensity of the brightest square is then recorded. This square does have depth, determined by the depth of field of the

objective lens and so is technically cuboid. For imaging diffraction limited foci, the numerical aperture of the lens is typically high, hence the depth of field is primarily determined by wave optics and will differ depending upon wavelength; our imaging system has a depth of field of 400-500 nm. Importantly, the z slice position of this square is also recorded, since the relative distance from the coverslip can have significant effects upon the measured fluorescence [17]. Selecting a 3D 'volume' that encloses all fluorescence above a given threshold is common in a number of commercial imaging software packages. Therefore, a second measurement is made by including the adjacent squares immediate above and below the brightest square (**Fig. 2D**). This 3D box (for example $3 \times 3 \times 3$ pixels) defines a volume that depends upon the spacing of the separate z stacks in the user's image and the depth of field of the objective lens. Finally, the mean fluorescence of the square in every slice in the z stack is also calculated (as in [32]).

It is important to subtract the fluorescence background from measurements of fluorescence in an image. In an ideal imaging system, the levels of background fluorescence are uniform across the field of view. However, since this ideal situation rarely applies and different cells may have different levels of background fluorescence, we chose to measure a local background measurement for each focus. We use an area that is two pixels outside of the brightest square and is two pixels wide (**Fig. 2C** and **D**). In addition, we also measure this same background area in the entire z stack, although we realise that, depending upon the z spacing, the fluorescence from a focus would contaminate this volume due to the point spread function in the z dimension. In summary, the ImageJ script makes three measurements of each focus and two background measurements. Each measurement is a mean value of the grey levels within each area or volume. Median measurements of both the brightest square and the background area are taken. Also, the integrated fluorescence from the 3D measurement is also calculated. The output of our script includes an image that indicates these foci and background regions in 2 dimensions (**Fig. 2E**). The tabulated results describe a number of details about each measurement. Each kinetochore measurement includes the mean and median values of the 2D measurement, the mean of the 3D measurement (box, as in **Fig. 2D**) and the mean of the whole stack. An example of the data output is shown in **Table S1**. The background region measurement for each focus includes the mean and median of the 2D measurement and the mean of the whole stack. Hence, with four different measures of kinetochore intensity and three measures of background intensity, there are twelve possible background-subtracted values that can be calculated for each focus. Here we use two different calculations of background-subtracted kinetochore foci intensity. First, the median background intensity is subtracted from the mean kinetochore intensity (both 2D), referred to as the 2D measurement. We use median background values rather than mean in case the background region overlaps neighboring foci, which would skew the mean. Second, for 3D measurements we use the 'box mean' of the kinetochore with the median 2D background subtracted. We have included a module in FociQuant that plots both, the center of mass of each focus, and the position of the peak of a Gaussian distribution; this positional information is included in the results table (e.g. see **Table S1**). This results table can be filtered in a number of ways, for example to eliminate dead cells, which would have a very high background fluorescence or to only select foci in one region of the image using the X, Y and Z coordinates.
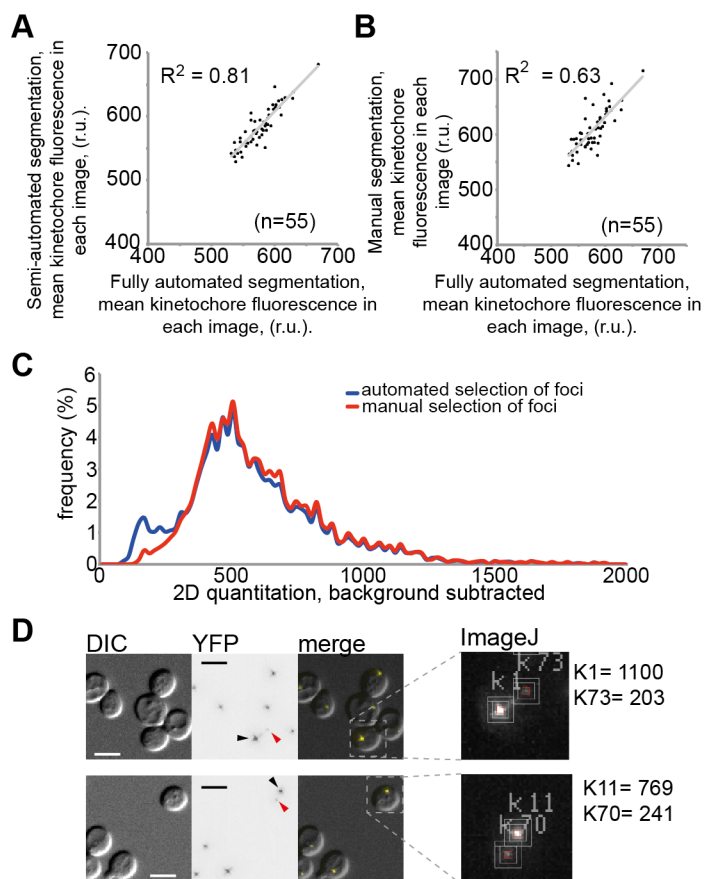

Figure 4. Comparing foci segmentation methods. A. The mean fluorescence intensities of kinetochores in each image are compared when using a fully automated segmentation (x axis) or semi-automated segmentation (y axis). Measurements are all made in 2D. **B.** The same comparison is made between fully automated segmentation (x axis) or manual segmentation (y axis). **C.** The distribution of foci fluorescence intensities is shown for automated segmentation of foci (blue, as in **Fig. 3C**) and manual selection of foci (red). The manual selection of foci avoids some of the weak foci that are sometimes found in wild-type cells. **D.** Two examples of these weak foci are highlighted with red arrowheads and shown in the graphical output of the ImageJ script. Black arrowheads indicate standard kinetochore foci. Scale bars are 5 µm and the (background subtracted, 2D) intensities of the highlighted foci are indicated.

Comparing 2D and 3D measurements

We compared the 2D, 3D and stack quantitation methods for a set of 55 sample images of a yeast strain (T37) in which the kinetochore is labeled with Dad4-YFP encoded at the genomic locus. Images were acquired as described in the Materials and Methods. An example of one of these images is shown in **Figure 1A**. We initially used FociQuant's automated segmentation approach to find the foci. In total 4981 foci were identified and quantified. We compared the 2D with 3D box quantitation and find that the methods are very well correlated (**Fig. 3A**). Our images contain 21 vertically-separated z planes spread over 7 µm and so are not ideal for whole stack measurements. However, we find good correlation between the whole stack and 2D measurements (**Fig. S1A** and **B**). The correlation between the different methods also extends to the mean intensities of foci from each of the 55 images (**Fig.**

3B). These data show that for relative quantitation of foci fluorescence, the 2D and 3D methods give equivalent data. The distribution of the foci intensities from the 2D and 3D quantitation are found to be similar (**Fig. 3C**). Members of the DAM1/DASH complex are relatively abundant kinetochore proteins [18], which makes the segmentation straightforward. To assess the ability of the methodology to measure weak foci, we quantified the fluorescence of Mif2, a lower abundance kinetochore protein. We find that Mif2-GFP foci are clearly visible with our normal imaging conditions using 200 msec exposure time (**Fig. 3D**), so we reduced the exposure time gradually to diminish the signal to noise ratio. We find that at < 50 msec exposure, FociQuant cannot readily identify the foci (**Fig. 3E**). These data confirm our expectation that foci quantitation, particularly using an automated approach, relies upon a sufficiently strong emission signal from the tagged protein, relative to the background noise in the image.

We next wished to ask whether the different segmentation methods would affect the average fluorescence intensities in these images. We used both the semi-automated and manual selection methods to quantify the fluorescence of foci in all of the 55 Dad4-YFP images and compared the results with those from the automated selection. The semi-automated method correlates well with the fully-automated method (**Fig. 4A**). The manual foci selection process should be the most precise since only genuine kinetochore foci are selected, however, it suffers from subjectivity, as the user may be biased to select only stereotypical kinetochore foci. Indeed we find only moderate correlation between the manual and automated methods (**Fig. 4B**). We noticed in the distributions of fluorescence intensities that a peak of low intensity foci was absent from the manual segmentation method (**Fig. 4C**). This class of foci have fluorescence that is less than half that of the normal kinetochores and examples of these weak foci are highlighted in **Figure 4D**. These foci may indicate lagging chromosomes or other aberrant kinetochore structures within a subset of wild-type cells.

The fluorescence intensity of kinetochore foci in unsynchronized cells (such as **Fig. 1A**) will contain kinetochore foci with a single complement of centromeres (1C) and a double complement (2C). 2C kinetochores arise after DNA replication in late S phase and early G2 phase. This would result in some S/G2 kinetochores with higher fluorescence [29]. The distribution of fluorescent intensities across the population of 4981 foci is relatively broad (**Fig. 3C**) with no obvious indication of two groups of foci (G1 vs G2). To assess the contribution of 2C kinetochores to the distribution of fluorescence intensity values, we used the manual selection method to quantify only separated metaphase kinetochores, which have a 1C DNA content. An example of these metaphase kinetochore is shown in **Figure 5A**, inset. The metaphase kinetochores do indeed produce a less variant fluorescence intensity (**Fig. 5A**).

Calibrating FociQuant software

To compare how the ImageJ script would compare with a commercial image analysis package we used Volocity software (Perkin Elmer) to quantify fluorescence in a set of images and compared the values with that obtained using our automated script. The details of the Volocity segmentation are provided in the supplementary information. Since the Volocity measurements are 3D, we compared them with our 3D measurements using FociQuant. We find that the two methods do correlate ($R^2 = 0.67$) for Dad4-YFP quantitation (**Fig. S1C**), but the correlation is less than we might have expected. This may be in part because all the images are of the same tagged protein (Dad4-YFP) in wild-type cells. Thus the differences between the images are relatively small and therefore more susceptible to small changes in quantitation.

To more reliably assess the ability of FociQuant to detect changes in the intensity of fluorescent foci, we compared both haploid and diploid cells with labeled kinetochore proteins. Since diploid cells have twice as many centromeres as haploids they can be expected to load twice the amount of kinetochore proteins. We used the automated method to assess both Mtw1 and Dad4 kinetochore protein levels in haploids and diploids and we used our automated FociQuant method. For Mtw1-YFP strains, we find ~70% increase in fluorescence from haploids to diploids (**Fig. 5B** and **Fig. S1D**). However, when we examined Dad4-YFP images we find that the fluorescence is only 40% higher in diploids than haploids (**Fig. 5C**). The same results were obtained using Volocity image analysis software (**Fig. S1E** and **F**). Additionally, a heterozygous diploid *DAD4-YFP/DAD4* strain contains less Dad4-YFP signal than a haploid (**Fig. 5C**). These latter data suggests either that Dad4-YFP does not compete effectively with untagged Dad4 for inclusion into the kinetochore or that the *DAD4-YFP* allele produces less Dad4 protein than the untagged allele. One possible reason the Dad4-YFP diploids do not have foci that are twice as bright as haploids may be that the automated segmentation method is less able to detect Dad4-YFP foci than Mtw1-YFP foci. To test this notion we manually selected Dad4-YFP foci in both haploids and diploids, but again the diploid cells only have 40% more Dad4 kinetochore fluorescence of haploids (**Fig. S1G**) The implications of these data are discussed later, but in summary the FociQuant software can detect the different levels of fluorescence between haploid and diploid cells.

A key concern with quantitative fluorescence imaging is the effect of fluorophore bleaching. If a significant proportion of the tagged protein is bleached, then the measurement of fluorescence will underestimate the true levels of fluorophores present in each focus. The rate of bleaching depends upon the fluorophore and its environment and is proportional to the excitation energy. Bleaching is a particular problem in confocal imaging, which uses high-energy excitation. The FociQuant software allows us to measure bleaching by quantifying fluorescence levels in cells that have been continuously exposed to excitation energy. Rapid bleaching can result in different z slices having different intensities due to progressive bleaching during the image acquisition. We imaged both Dad4-YFP and Mif2-GFP with continuous exposure to LED excitation for approximately 9 minutes, with a z stack of images captured every 12 seconds (each z stack takes approximately 3 seconds to capture). Individual foci were quantified for each time point using the automated segmentation method. The resulting bleaching curves show different rates of bleaching for these two proteins (**Fig. 5D**). Hence, FociQuant can be used to assess bleaching rates for specific tagged proteins that form foci. In this case, the effect of bleaching should be small within the 3 second acquisition time used for the images shown.

mad1Δ mutants

The purpose of our FociQuant software is to enable high-throughput analysis. To test the ability of FociQuant to detect mutations that impact the kinetochore, we chose to look at mutants in the mitotic checkpoint gene *MAD1*. Mad1 binds to kinetochores in response to phosphorylation of Bub1 and aids the conversion of Mad2 from an 'open' to a 'closed' form, which is a key step in checkpoint activation [33, 34]. Mutants of *MAD1* have an abrogated checkpoint and therefore may proceed through mitosis without all their chromosomes correctly attached to the mitotic spindle. This leads to a chromosomal instability phenotype [35, 36]. We captured images of both wild-type and *mad1Δ* cells containing Dad4-YFP and used the automated analysis method to compare the fluorescence intensity of their kinetochore foci. We find that *mad1Δ*

cells have a broader distribution of kinetochore fluorescence intensities than wild type (**Fig. 6A**), consistent with the aberrant kinetochore foci that are observed in many cells (**Fig. 6B**). Overall we detect an increase in the mean kinetochore fluorescence in *mad1Δ* cells (**Fig. 6C**). Thus, our methodology readily detects the changes produced by checkpoint mutations, and could therefore be used to identify similar changes produced by other genetic changes that would lead to a chromosomal instability phenotype.

2 channel analysis

Since the software is modular it is possible to build in the ability to analyze a second fluorescence channel. To demonstrate this we have used such a "2 channel" analysis of cells tagged with both Dad4-YFP and Spc42-RFP. Spc42 is a spindle pole body protein and hence marks the microtubule organizing center in yeast. We include a proximity threshold, that the user defines, to search within a defined number of pixels of the primary focus for a focus in the second channel. Hence, only RFP foci within a set number of pixels of the YFP focus will be analyzed. The second channel is quantified as for the first channel and the positions of the second channel foci are marked on the graphical output (**Fig. 6D**). An example of the typical tabulated output is shown in **Table S2**. The scripts for 2 color imaging are also freely available to download (https://sourceforge.net/projects/fociquantitation/files/).
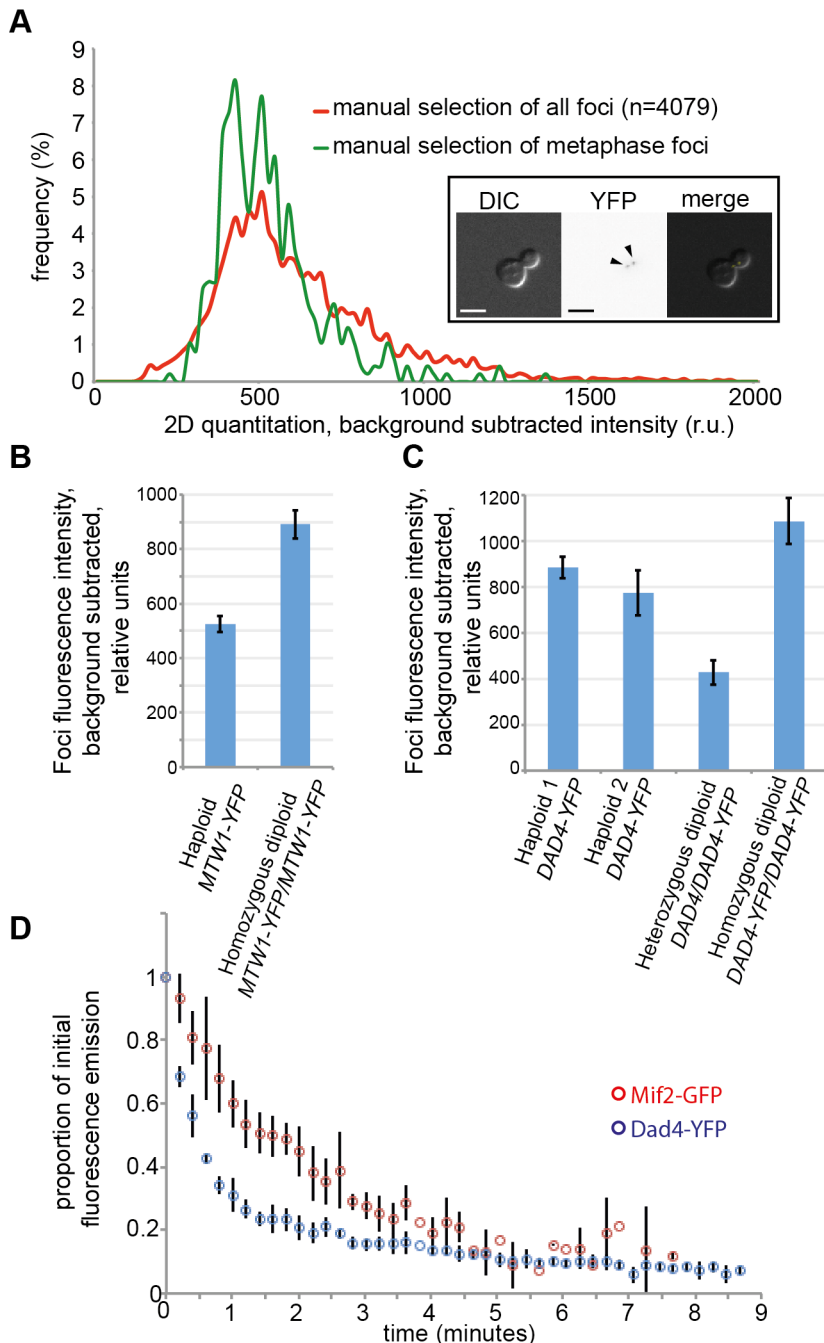
Figure 5. A. Effects of cell cycle and a comparison with commercial software. A comparison of the distribution of Dad4-YFP kinetochore fluorescence intensities derived from manual selection of all kinetochore foci (red) with manual selection of kinetochores that are in metaphase (green). The metaphase kinetochores have a narrower distribution (mean = 509 r.u., n = 480, standard deviation = 153 r.u.) compared with all foci (mean = 605 r.u., n = 4087, standard deviation = 269 r.u.). The inset image shows a stereotypical metaphase pair of kinetochores, the scale bar is 5 μm. **B.** The mean fluorescence intensity of Mtw1-YFP foci in both haploids and diploids is shown for FociQuant automated analysis, the error bars indicate one standard deviation. **C.** The mean fluorescence intensity of Dad4-YFP foci in both haploids and diploids is shown for FociQuant automated analysis, the error bars indicate one standard deviation. **D.** The foci fluorescence of six Mif2-GFP foci and six Dad4-YFP foci are shown over time with continual fluorescence exci- tation; the fluorescence data are normalized to the starting fluorescence measurement, which is set to the value 1. The error bars indicate one standard deviation. The foci were identified using the automated segmentation protocol and at later time points some foci are not detected hence the absence of error bars on some time points.
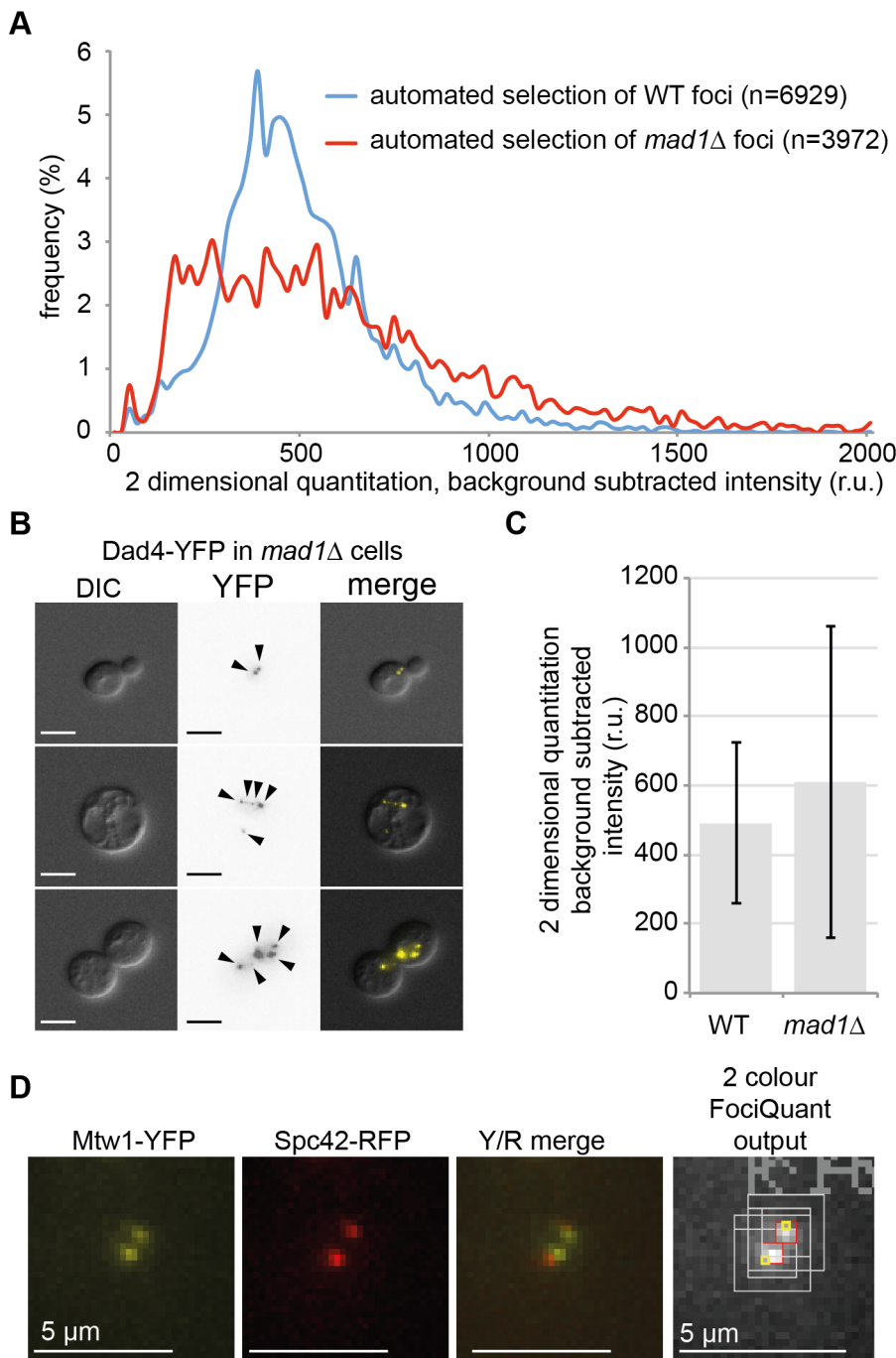
Figure 6. The fluorescence intensity of kineto-chores in *mad1Δ* cells and 2 colour analysis. A. The distribution of foci fluorescence intensities of a new set of wild-type images (blue) are compared with those of *mad1Δ* cells (red). All measurements are automated 2D analysis. **B.** Examples of *mad1Δ* cells with normal (top) or aberrant (middle and bottom) kinetochore foci are shown, scale bar is 5 µm. **C.** The average kinetochore intensity of *mad1Δ* cells is higher than wild type (Students *t*-test P < 0.0001), the error bars indicate standard deviation of the mean. **D.** An example of 2-colour measurement is shown for Dad4-YFP, Spc42-RFP. The position of the centre of the second channel measurement is indicated on the graphical output with a yellow box. The scale bar is 5 µm, the tabulated quantitation of these two yellow and two red foci are shown in **Table S2**.

DISCUSSION

We have developed a software tool, FociQuant, that enables high-throughput quantitative analysis of the fluorescence levels of foci in cells. The software is freely available and runs on the popular ImageJ platform. The modular nature of FociQuant and extensive line-by-line documentation allow the script to be modified with new functions or new image formats as required. The software provides various outputs of quantitation including both 2D and 3D analysis with a number of background correction possibilities. The tabulated results data can be mined to extract, for example, dead cells that have a high fluorescence background or to enrich for metaphase cells. We use this methodology to compare different methods of foci quantitation and show that they correlate well with each other. We also compare FociQuant with a com-

mercial software package for fluorescence quantitation and find good correlation between the methods. The aim of FociQuant is to enable high-throughput analysis of images of kinetochore foci to identify per-turbations that affect kinetochore protein levels. Initially, we compared haploid and diploid strains encoding the kinetochore proteins Mtw1-YFP and Dad4-YFP. FociQuant and Volocity software consistently detect a ~70% increase in fluorescence intensity of diploid Mtw1-YFP kineto-chore foci, compared with haploid strains. However, Dad4-YFP shows a more modest increase in fluorescence (~40%). There are a number of possible reasons for this. First, it is possible that the addition of the YFP tag to Dad4 causes a perturbation in the structure of the kineto-chore, although we do not see any obvious mitotic growth defects in *DAD4-YFP* strains. The observation that heterozygous diploids appear to selectively exclude Dad4-YFP from the kinetochore may support the

idea that the tagged protein is not equivalent to an untagged version. We note that Dad4-YFP fluorescence shows a considerable variation between cells (**Fig. 5A**); the coefficient of variation of automatically selected haploid foci fluorescence is 0.49 compared with 0.32 for Mtw1. The high Dad4-YFP variance may be a result of the fluorescent tag. Second, there may be rapid turnover of kinetochore bound Dad4-YFP, especially in diploids, and coupled with slow fluorophore maturation, the fluorescence signal may no longer correlate with protein numbers. However, experiments with structural kinetochore proteins do not support the notion of rapid turnover [18, 29, 37]. Although, these data could be interpreted to indicate that Dad4 is not loaded stoichiometrically with the rest of the DAM1/DASH complex in diploid cells, this seems an unlikely option. Previous studies with DAM1/DASH proteins show that they work together as part of heterodecameric complex [38], although with some flexibility as to their stoichiometry [18]. The DAM1/DASH proteins are thought to form a ring around microtubules [38, 39] and they are essential. Consequently we would expect the members of the DAM1/DASH complex to scale with the other kinetochore proteins. Finally, it is possible that a proportion of the Dad4-YFP in the cell has the YFP moiety improperly folded, resulting in a pool of non-fluorescent Dad4-YFP. This notion could explain the high degree of cell to cell variation in fluorescence intensity seen with Dad4-YFP.

We show that our methodology is sufficient to identify changes in kinetochore fluorescence produced by a mutation in the checkpoint gene *MAD1*. Checkpoint mutants proceed through mitosis even if chromosomes are not correctly attached to the mitotic spindle. The automated analysis of the kinetochore fluorescence of *mad1Δ* cells indicated a large range of fluorescence intensities from very weak foci to highly-fluorescent foci. This observation indicates altered Dad4 protein levels, which may be the result of chromosomal instability or checkpoint dysfunction that are characteristic of *mad1Δ* cells [35, 36]. This analysis shows that the software can detect changes in kinetochore fluorescence in mutants that affect chromosome segregation using the fluorescence intensities or distribution of intensities (**Fig. 6**). It should be pointed out that our cell cultures were not synchronized to a specific point in the cell cycle. Since kinetochore fluorescence increases as cells replicate their centromeres in S phase, late S/G2 cells would be expected to have higher levels of fluorescence at kinetochores. Additionally, cells in early mitosis may start to separate their kinetochores but by a distance that is less than the diffraction limit, in which case two foci would be quantified as one. Thus the cell cycle stage of cultures could influence the foci fluorescence.

Since FociQuant is modular and flexible it can be adapted to different types of cellular foci and provides different types of fluorescence measurements. For example, a second channel can be measured to compare the levels and location of a second kinetochore or spindle protein within the same cells, as indicated in **Figure 6D**. We have built a software module to plot the position of foci at a resolution beyond the diffraction limit (using Gaussian fitting of diffraction limited spots), the software could determine the spatial separation of two cellular proteins in high-throughput data. Alternatively, the script could be adapted to identify different shapes such as lines consistent with microtubules. The software could also be used to screen for split GFP association or potentially for FRET studies both of which have been useful for studying the yeast kinetochore [40, 41]. Consequently, the methodology outlined here provides a robust tool for relative quantitation of fluorescence signals from large numbers of foci and has the potential to be used in numerous applications beyond simple quantitation.

References

1. Huh W, Falvo JV, Gerke LC, Carroll AS, Howson RW, et al. (2003) Global analysis of protein localization in budding yeast. Nature 425: 686-691. doi: 10.1038/nature02026. PMID: 14562095

2. Tkach JM, Yimit A, Lee AY, Riffle M, Costanzo M, et al. (2012) Dissecting DNA damage response pathways by analysing protein localization and abundance changes during DNA replication stress. Nat Cell Biol 14: 966-976. doi: 10.1038/ncb2549. PMID: 22842922

3. Chong YT, Koh JLY, Friesen H, Duffy K, Cox MJ, et al. (2015) Yeast Proteome Dynamics from Single Cell Imaging and Automated Analysis. Cell 161: 1413-1424. doi: 10.1016/j.cell.2015.04.051. PMID: 26046442

4. Lisby M, Rothstein R, Mortensen UH (2001) Rad52 forms DNA repair and recombination centers during S phase. Proc Natl Acad Sci U S A 98: 8276-8282. doi: 10.1073/pnas.121006298. PMID: 11459964

5. Alvaro D, Lisby M, Rothstein R (2007) Genome-wide analysis of Rad52 foci reveals diverse mechanisms impacting recombination. PLoS Genet 3: doi: 10.1371/journal.pgen.0030228. PMID: 18085829

6. Biggins S (2013) The composition, functions, and regulation of the budding yeast kinetochore. Genetics 194: 817-846. doi: 10.1534/genetics.112.145276. PMID: 23908374

7. Cheeseman IM (2014) The kinetochore. In: Cold Spring Harb Perspect Biol 6: a015826

8. Westermann S, Drubin DG, Barnes G (2007) Structures and functions of yeast kinetochore complexes. Annu Rev Biochem 76: 563-591. doi: 10.1146/annurev.biochem.76.052705.160607. PMID: 17362199

9. Crasta K, Ganem NJ, Dagher R, Lantermann AB, Ivanova EV, et al. (2012) DNA breaks and chromosome pulverization from errors in mitosis. Nature 482: 53-58. doi: 10.1038/nature10802. PMID: 22258507

10. Schliekelman M, Cowley DO, O'Quinn R, Oliver TG, Lu L, et al. (2009) Impaired Bub1 function *in vivo* compromises tension-dependent checkpoint function leading to aneuploidy and tumorigenesis. Cancer Res 69: 45-54. doi: 10.1158/0008-5472.CAN-07-6330. PMID: 19117986

11. Sheltzer JM, Blank HM, Pfau SJ, Tange Y, George BM, et al. (2011) Aneuploidy drives genomic instability in yeast. Science 333: 1026-1030. doi: 10.1126/science.1206412. PMID: 21852501

12. Stirling PC, Bloom MS, Solanki-Patil T, Smith S, Sipahimalani P, et al. (2011) The complete spectrum of yeast chromosome instability genes identifies candidate CIN cancer genes and functional roles for ASTRA complex components. PLoS Genet 7: doi: 10.1371/journal.pgen.1002057. PMID: 21552543

13. Sun W, Yao L, Jiang B, Guo L, Wang Q (2014) Spindle and kinetochore-associated protein 1 is overexpressed in gastric cancer and modulates cell growth. Mol Cell Biochem 391: 167-174. doi: 10.1007/s11010-014-1999-1. PMID: 24627241

14. Ryan SD, Britigan EMC, Zasadil LM, Witte K, Audhya A, et al. (2012) Up-regulation of the mitotic checkpoint component Mad1 causes chromosomal instability and resistance to microtubule poisons. Proc Natl Acad Sci U S A 109: 2205-14. doi: 10.1073/pnas.1201911109. PMID: 22778409

15. Sotillo R, Hernando E, Díaz-Rodríguez E, Teruya-Feldstein J, Cordón-Cardo C, et al. (2006) Mad2 overexpression promotes aneuploidy and tumorigenesis in mice. Cancer Cell 11: 9-23. doi: 10.1016/j.ccr.2006.10.019. PMID: 17189715

16. Tomonaga T, Matsushita K, Ishibashi M, Nezu M, Shimada H, et al. (2005) Centromere protein H is up-regulated in primary human colorectal cancer and its overexpression induces aneuploidy. Cancer Res 65: 4683-4689. doi: 10.1158/0008-5472.CAN-04-3613. PMID: 15930286

17. Joglekar AP, Salmon ED, Bloom KS (2008) Counting kinetochore protein numbers in budding yeast using genetically encoded fluorescent proteins. Methods Cell Biol 85: 127-151. doi: 10.1016/S0091-679X(08)85007-8. PMID: 18155462

18. Joglekar AP, Bouck DC, Molk JN, Bloom KS, Salmon ED (2006) Molecular architecture of a kinetochore-microtubule attachment site. Nat Cell Biol 8: 581-585. doi: 10.1038/ncb1414. PMID: 16715078

19. Lawrimore J, Bloom KS, Salmon ED (2011) Point centromeres contain more than a single centromere-specific Cse4 (CENP-A) nucleosome. J Cell Biol 195: 573-582. doi: 10.1083/jcb.201106036. PMID: 22084307

20. Cieslinski K, Ries J (2014) The yeast kinetochore - structural insights from optical microscopy. Curr Opin Chem Biol 20: 1-8. doi: 10.1016/j.cbpa.2014.03.020. PMID: 24763395

21. Zou H, Rothstein R (1997) Holliday junctions accumulate in replication mutants via a RecA homolog-independent mechanism. Cell 90: 87-96. PMID: 9230305

22. Thomas BJ, Rothstein R (1989) The genetic control of direct-repeat recombination in Saccharomyces: the effect of rad52 and rad1 on mitotic recombination at GAL10, a transcriptionally regulated gene. Genetics 123: 725-738. PMID: 2693208

23. Brachmann CB, Davies A, Cost GJ, Caputo E, Li J, et al. (1998) Designer deletion strains derived from Saccharomyces cerevisiae S288C: a useful set of strains and plasmids for PCR-mediated gene disruption and other applications. Yeast 14: 115-132. doi: 10.1002/(SICI)1097-0061(19980130)14:2<115::AID-YEA204>3.0.CO;2-2. PMID: 9483801

24. Sherman F (2002) Getting started with yeast. Methods Enzymol 350: 3-41.

25. Winzeler EA, Shoemaker DD, Astromoff A, Liang H, Anderson K, et al. (1999) Functional characterization of the S. cerevisiae genome by gene deletion and parallel analysis. Science 285: 901-906. PMID: 10436161

26. Schneider CA, Rasband WS, Eliceiri KW (2012) NIH Image to ImageJ: 25 years of image analysis. Nat Methods 9: 671-675. PMID: 22930834

27. Sluder G, Wolf DE (2013) Digital microscopy. In: Digital microscopy. San Diego: Academic Press 672 p.

28. Cheeseman IM, Anderson S, Jwa M, Green EM, Kang, J, et al. (2002) Phospho-regulation of kinetochore-microtubule attachments by the Aurora kinase Ipl1p. Cell 111: 163-172. PMID: 12408861

29. Wisniewski J, Hajj B, Chen J, Mizuguchi G, Xiao H, et al. (2014) Imaging the fate of histone Cse4 reveals de novo replacement in S phase and subsequent stable residence at centromeres. Elife 3: doi: 10.7554/eLife.02203. PMID: 24844245

30. Carpenter AE, Jones TR, Lamprecht MR, Clarke C, Kang IH, et al. (2006) CellProfiler: image analysis software for identifying and quantifying cell phenotypes. Genome Biol 7: doi: 10.1186/gb-2006-7-10-r100. PMID: 17076895

31. Herbert AD, Carr AM, Hoffmann E (2014) FindFoci: a focus detection algorithm with automated parameter training that closely matches human assignments, reduces human inconsistencies and increases speed of analysis. PLoS One 9: doi: 10.1371/journal.pone.0114749. PMID: 25478967

32. Wu JQ, McCormick CD, Pollard TD (2008) Chapter 9: Counting proteins in living cells by quantitative fluorescence microscopy with internal standards. Methods Cell Biol 89: 253-273. doi: 10.1016/S0091-679X(08)00609-2. PMID: 19118678

33. London N, Biggins S (2014) Mad1 kinetochore recruitment by Mps1-mediated phosphorylation of Bub1 signals the spindle checkpoint. Genes Dev 28: 140-152. doi: 10.1101/gad.233700.113. PMID: 24402315

34. Musacchio A, Salmon ED (2007) The spindle-assembly checkpoint in space and time. Nat Rev Mol Cell Biol 8: 379-393. doi: 10.1038/nrm2163. PMID: 17426725

35. Warren CD, Brady DM, Johnston RC, Hanna JS, Hardwick KG, et al. (2002) Distinct chromosome segregation roles for spindle checkpoint proteins. Mol Biol Cell 13: 3029-3041. doi: 10.1091/mbc.E02-04-0203. PMID: 12221113

36. Doncic A, Ben-Jacob E, Einav S, Barkai N (2009) Reverse engineering of the spindle assembly checkpoint. PLoS One 4: doi: 10.1371/journal.pone.0006495. PMID: 19652707

37. Pearson CG, Yeh E, Gardner M, Odde D, Salmon ED, et al. (2004) Stable kinetochore-microtubule attachment constrains centromere positioning in metaphase. Curr Biol 14: 1962-1967. doi: 10.1016/j.cub.2004.09.086. PMID: 15530400

38. Miranda JJL, De Wulf P, Sorger PK, Harrison SC (2005) The yeast DASH complex forms closed rings on microtubules. Nat Struct Mol Biol 12: 138-143. doi: 10.1038/nsmb896. PMID: 15640796

39. Westermann S, Avila-Sakar A, Wang H, Niederstrasser H, Wong J, et al. (2005) Formation of a dynamic kinetochore- microtubule interface through assembly of the Dam1 ring complex. Mol Cell 17: 277-290. doi: 10.1016/j.molcel.2004.12.019. PMID: 15664196

40. Aravamudhan P, Felzer-Kim I, Joglekar AP (2013) The budding yeast point centromere associates with two Cse4 molecules during mitosis. Curr Biol 23: 770-774. doi: 10.1016/j.cub.2013.03.042. PMID: 23623551

41. Aravamudhan P, Felzer-Kim I, Gurunathan K, Joglekar AP (2014) Assembling the protein architecture of the budding yeast kinetochore-microtubule attachment using FRET. Curr Biol 24: 1437-1446. doi: 10.1016/j.cub.2014.05.014. PMID: 24930965

Supplementary information

Supplementary Text

Figure S1. Comparison of quantitation methods for fluorescent foci

Table S1. Output tabulated data from FociQuant

Table S2. Output tabulated data from 2 color FociQuant

Supplementary information of this article can be found online at http://www.jbmethods.org.